AFWAL-TR-88-2136

VORTEX-TRANSPORT ELEMENT SIMULATION OF A CONFINED MIXING LAYER

P. Givi

Flow Research Company
Applied Mechanics Division
21414 - 68th Avenue South
Kent, Washington, 98032

November 1988

Final Report for Period September 1987 - March 1988

AERO PROPULSION AND POWER LABORATORY
AIR FORCE WRIGHT AERONAUTICAL LABORATORIES
AIR FORCE SYSTEMS COMMAND
WRIGHT-PATTERSON AIR FORCE BASE, OHIO 45433-6563

NOTICE

When Government drawings, specifications, or other data are used for any purpose other than in connection with a definitely Government-related procurement, the United States Government incurs no responsibility or any obligation whatsoever. The fact that the Government may have formulated or in any way supplied the said drawings, specifications, or other data, is not to be regarded by implication, or otherwise in any manner construed, as licensing the holder, or any other person or corporation; or as conveying any rights or permission to manufacture, use, or sell any patented invention that may in any way be related thereto.

This report has been reviewed by the Office of Public Affairs (ASD/PA) and is releasable to the National Technical Information Service (NTIS). At NTIS, it will be available to the general public, including foreign nations.

This technical report has been reviewed and is approved for publication.

Thomas Jackson

THOMAS JACKSON
Project Engineer

Charles L Delaney

CHARLES L. DELANEY
Fuels Branch

FOR THE COMMANDER

Benito P. Botteri

BENITO P. BOTTERI, Assistant Chief
Fuels and Lubrication Division
Aero Propulsion Laboratory

Accession For	
NTIS GRA&I	X
DTIC TAB	☐
Unannounced	☐
Justification	
By	
Distribution/	
Availability Codes	
Dist	Avail and/or Special
A-1	

QUALITY INSPECTED 1

If your address has changed, if you wish to be removed from our mailing list, or if the addressee is no longer employed by your organization please notify AFWAL/POSF , Wright-Patterson AFB, OH 45433- 6563 to help us maintain a current mailing list.

Copies of this report should not be returned unless return is required by security considerations, contractual obligations, or notice on a specific document.

Unclassified
SECURITY CLASSIFICATION OF THIS PAGE

REPORT DOCUMENTATION PAGE

Form Approved OMB No 0704-0188

1a. REPORT SECURITY CLASSIFICATION: Unclassified	1b. RESTRICTIVE MARKINGS
2a. SECURITY CLASSIFICATION AUTHORITY	3. DISTRIBUTION/AVAILABILITY OF REPORT: Approved for Public Release; Distribution is Unlimited
2b. DECLASSIFICATION/DOWNGRADING SCHEDULE	
4. PERFORMING ORGANIZATION REPORT NUMBER(S): Flow Research Report No. 442	5. MONITORING ORGANIZATION REPORT NUMBER(S): AFWAL-TR-88-2136
6a. NAME OF PERFORMING ORGANIZATION: Flow Research, Inc. / 6b. OFFICE SYMBOL (If applicable)	7a. NAME OF MONITORING ORGANIZATION: Aero Propulsion & Power Laboratory (AFWAL/POSF) Air Force Wright Aeronautical Laboratories
6c. ADDRESS (City, State, and ZIP Code): 21414 - 68th Avenue South, Kent, WA 98032	7b. ADDRESS (City, State, and ZIP Code): Wright-Patterson Air Force Base, Oh 45433-6563
8a. NAME OF FUNDING/SPONSORING ORGANIZATION: Department of the Air Force / 8b. OFFICE SYMBOL (If applicable): AFWAL/POSF	9. PROCUREMENT INSTRUMENT IDENTIFICATION NUMBER: Contract No. F33615-87-C-2790
8c. ADDRESS (City, State, and ZIP Code): Wright-Patterson Air Force Base, OH 45433	10. SOURCE OF FUNDING NUMBERS: PROGRAM ELEMENT NO. 65502F; PROJECT NO. 3005; TASK NO 20; WORK UNIT ACCESSION NO. 90

11. TITLE (Include Security Classification)
Vortex-Transport Element Simulation of a Confined Mixing Layer

12. PERSONAL AUTHOR(S)
Peyman Givi

13a. TYPE OF REPORT	13b. TIME COVERED	14. DATE OF REPORT (Year, Month, Day)	15. PAGE COUNT
Final	FROM 9-87 TO 3-88	1988 November	42

16. SUPPLEMENTARY NOTATION
This is a Small Business Innovation Research Program Report, Phase I

17. COSATI CODES		
FIELD	GROUP	SUB-GROUP
21	01	
21	02	

18. SUBJECT TERMS (Continue on reverse if necessary and identify by block number)
Vortex Method, Turbulent Mixing; Chemical Reaction; Numerical Simulation; Scalar Transport; Combusting shear layers, (rdc) A

19. ABSTRACT (Continue on reverse if necessary and identify by block number)

An improved vortex-transport element numerical scheme has been employed to simulate the spatial evolution of a two-dimensional planar, constant density mixing layer formed behind a splitter plate configuration. This scheme uses vortex elements to discretize the region of high vorticity, and transport elements to discretize the region of high scalar gradients. This improved vortex method offers a method of accurately resolving the areas of high strain by redistributing the neighboring elements within those regions.

The resulting scheme has been used to simulate the convective transport of a conserved scalar variable in the shear layer, and the results show favorable agreement with experimental data for the mean and the rms values of the scalar quantity. The effects of harmonic forcing are shown to accelerate the mechanism of the rollup and pairing within the domain, which results in an increase in the convolution of the surfaces. This would be of crucial interest to the problem of active combustion control in a reacting mixing layer simulation.

20. DISTRIBUTION/AVAILABILITY OF ABSTRACT	21. ABSTRACT SECURITY CLASSIFICATION
☒ UNCLASSIFIED/UNLIMITED ☐ SAME AS RPT ☐ DTIC USERS	Unclassified

22a. NAME OF RESPONSIBLE INDIVIDUAL	22b. TELEPHONE (Include Area Code)	22c. OFFICE SYMBOL
Thomas A. Jackson	(513) 255-6462	AFWAL/POSF

DD Form 1473, JUN 86 — Previous editions are obsolete. SECURITY CLASSIFICATION OF THIS PAGE

Unclassified

Vortex-Transport Element Simulation of a Confined Mixing Layer

by

Peyman Givi
Flow Research Company
Kent, Washington 98032

ABSTRACT

An improved vortex-transport element numerical scheme has been employed to simulate the spatial evolution of a two-dimensional planar, constant density mixing layer formed behind a splitter plate configuration. This scheme uses vortex elements to discretize the region of high vorticity, and transport elements to discretize the region of high scalar gradients. This improved vortex method offers a method of accurately resolving the areas of high strain by redistributing the neighboring elements within those regions.

The resulting scheme has been used to simulate the convective transport of a conserved scalar variable in the shear layer, and the results show favorable agreement with experimental data for the mean and the rms values of the scalar quantity. The effects of harmonic forcing are shown to accelerate the mechanism of the rollup and pairing within the domain, which results in an increase in the convolution of the surfaces. This would be of crucial interest to the problem of active combustion control in a reacting mixing layer simulation.

1. INTRODUCTION

Nonpremixed turbulent reacting flows have been the subject of extensive experimental and theoretical investigations during recent years [for reviews, see Bilger (1976, 1980) and Givi (1984)]. In most of the theoretical work, turbulence models are used to close a system of averaged transport equations, which describes the statistical behavior of the aerothermodynamical variables. Moment methods (Donaldson and Varma, 1976), eddy break-up and mixing-controlled models (Givi et al., 1984a), flame sheet approximation (Bilger, 1980), assumed probability density function (PDF) shape methods (Lockwood and Naguib, 1975), solutions based on modeled joint PDF of scalar quantities (Givi et al., 1984b, Nguyen and Pope, 1984) and based on modeled joint PDF of scalar and velocity (Pope and Correa, 1987) are examples in which turbulence modeling have been used for the closure of equations governing the statistical quantities. Much effort has gone into constructing accurate models and in obtaining results that are in agreement with experimental measurements. However, in complex systems, modeling is difficult because of our lack of knowledge on the detailed dynamics of the flow. Furthermore, since most of the interesting dynamical behavior of the flow is modeled a priori, such features are not exhibited from the results of numerical computations based on turbulence models, and thus cannot advance our understanding of turbulent combustion.

The progress in numerical methods and the availability of supercomputers have had a major impact on turbulence research. Improved accuracy of the numerics and increased storage and computational speed have made it possible to solve the appropriate transport equations governing turbulent combustion directly without the need for modeling over some limited parameter range. Such nearly "model-free" simulations, in comparison with calculations utilizing turbulence models, have the advantage that the dominant physics of the problem

is not modeled a priori but is recovered directly from the computed results. These results can be used to understand many important mechanisms of turbulent transport and its direct influence on chemical reactions. Furthermore, since the instantaneous behavior of the variables are known at all points and at all times, accurate simulations offer a good method of probing the flow when experimental techniques may fail. There are, however, some limitations on the range of turbulent scales that can be resolved accurately by model-free simulations. Therefore, there is a need to validate the results of the simulations by a direct comparison with experimental measurements. With such validations, ab initio predictions can ultimately be a reality.

Numerical methods have been used in a variety of forms for the simulation of turbulent flows in complex configurations. A recent survey can be found in review articles (Oran and Boris, 1987). In reacting flow, three approaches are used: (1) finite difference methods, (2) spectral methods, and (3) vortex methods. In the first approach, the variables are defined on a grid and the transport equations are approximated by discretizing the derivatives on the grid nodes. Examples of this approach can be found in the work of Corcos and Sherman (1984), who used a projection method to study the temporal evolution of a periodic shear layer, and in Grinstein et al. (1985), who used a flux-corrected transport scheme to simulate the development of coherent structures in a two-dimensional spatially evolving shear layer and examined their effect on mixing.

In spectral methods, the variables are expanded in a series of harmonic functions that satisfy the differential equations on a number of collocation points. Riley et al. (1986) used a pseudo-spectral scheme to study a three-dimensional temporally-evolving reacting mixing layer assuming a constant reaction rate, constant density, and no heat release. McMurtry et al. (1986)

considered the effects of the chemical heat release on the fluid dynamics of a two-dimensional mixing layer for a constant reaction rate. The interplay between fluid dynamics and the chemical reaction is investigated under these conditions. Givi et al. (1987) used the same method to compute a two-dimensional mixing layer with an Arrhenius chemical reaction and constant density to assess the effects of large coherent structure on the local extinction of the flame. Extension to spatially-growing layers was initiated by Givi and Jou (1988) using a hybrid psendo-spectral second order finite difference scheme. In all cases, the Reynolds number was kept at small values, 0(100), limited by the grid resolution and the number of harmonic modes.

In the third approach, vortex methods are used. These schemes are grid free, the transport of the variables takes place in a Lagrangian form, and the solution is not restricted by the geometry of the confinement. Therefore, they can provide accurate simulations for high Reynolds number, spatially growing flows. Moreover, vortex methods optimize the computational efforts by distributing computational elements around regions of high vorticity. The application of the method in thin premixed flame calculations with a finite density jump has been reported by Ghoniem et al. (1982) and Sethian (1984), among others. In these calculations, the vortex method was employed to compute the flow field, and the dynamic effect of combustion was represented by the propagation of a thin interface at the laminar burning velocity acting as a volumetric source.

Vortex methods were also used in simulating diffusion flames in connection with a finite-difference approach for the treatment of the scalar variables. Ashurst and Barr (1982) used the vortex method to compute the hydrodynamic field and an Eulerian flux-corrected transport algorithm to compute the diffusion and convection of a conserved Shvab-Zeldovich scalar approximating

the shape and convolution of the flame in the limit of infinitely fast chemical reaction. Lin and Pratt (1987) used the random vortex method to simulate the large-scale motion and a Monte-Carlo method to calculate the time-dependent probability density function of the scalar quantities for both gaseous and aqueous mixing layers. The PDF transport equation, however, required a closure model for the molecular mixing term. The application of Lagrangian methods for reactive flow was initiated by Ghoniem and Givi (1987), who used vortex-scalar methods for the simulations of a reacting mixing layer at low heat release. In that work, vortex methods were used for hydrodynamic simulations, whereas scalar methods were used to simulate the scalar (temperature and concentration) variables. The results of that work, although very encouraging, indicated that one would need an excessive number of scalar elements to simulate the scalar variables accurately. Further, the results indicated that since the elements (both the vortex and the scalar) tend to evacuate regions of high local strain, better numerical methods are required to simulate such flows more accurately.

From this short review, it is clear that numerical simulations have played an important role in elucidating the physics of turbulent reacting flows, and that there is a continuing need for more direct simulations in order to better explain some of the interesting physical phenomena that have been observed in laboratory experiments.

In this work, we extend the vortex methods to study a nonreacting spatially developing mixing layer. This is an essential step before dealing with the problem of chemical reactions. The vortex transport element method is developed to treat both the hydrodynamic and the scalar field in a Lagrangian sense. The fact that a chemical reaction is truly a Lagrangian process, i.e., it occurs when the particles (or macroscopic elements) interact as they flow, motivate the implementation of Lagrangian methods for simulations of high

Reynolds number reacting flows. The method is capable of handling a wide variety of initial and boundary conditions and is not limited to simple flow boundaries. In this report, we concentrate on the formulation of the model and the numerical schemes, and present some preliminary validation studies and interpretations of the results.

In the next section, the geometrical configuration of a spatially-evolving mixing layer is presented. In this section, the formulation of the vortex method is given, and some sample results of the vorticity field are presented. These results are used to express the shortcomings associated with vortex methods. In Section 3, the improved vortex methods are explained together with a description of the transport-element methods. This report ends in Section 4, where summary and conclusions are given.

2. VORTEX METHODS

Consider a two-dimensional flow behind a splitter-plate configuration, as shown in Figure 1. In this figure, the velocity on the top stream is equal to U1 and the velocity of the low-speed bottom stream is U2. The flow is assumed incompressible, and the effects of boundary layer near the top and bottom walls are neglected.

Vortex methods are usually very appropriate to be used for the simulations of this type of flow since, at least initially, the vorticies are concentrated within a small region of the flow. The formulation of this scheme, which has been explained in detail in the literature, will be only briefly summarized here for the purpose of continuity with the next section.

The unsteady hydrodynamic transport equations are nondimensionalized with respect to the channel height H and the velocity difference across the layer Delta U = U1-U2. Under these conditions, the normalized equations are

$$\frac{\partial \omega}{\partial t} + \underline{u} \cdot \nabla \omega = \frac{1}{Re} \nabla^2 \omega \tag{1}$$

$$\nabla^2 \xi = -\omega \tag{2}$$

where ω is the vorticity, ξ is the stream function and U and V are the x and y components of the vorticity, i.e.,

$$U = \frac{\partial \xi}{\partial y} \tag{3}$$

$$V = -\frac{\partial \xi}{\partial x} \tag{4}$$

To implement the vortex method, the vorticity field is represented by a finite number of vortex elements of finite cores:

$$\omega(\underline{x}, t) = \sum Ti/\delta^2 \; f(\underline{x} - \underline{x}i) \tag{5}$$

where Ti is the circulation of a vortex element and δ is the core radius, while $\underline{x}i$ is the center of the element. f represents the vorticity distribution associated with a vortex element, or the core function (Chorin, 1973; Hald, 1979; and Beale and Majda, 1982). The velocity field is obtained by solving Equation (2) using the discrete vorticity distribution:

$$\underline{u} = \sum Ti \; K(\underline{x} - \underline{x}i) + Up \tag{6}$$

where $K(\underline{x}) = -(y,-x)/r^2$ is the kernel of the Poisson equation, $K(x) = \int r \; f(r) \; dr$ is the circulation within r, and $r = |x|$. Up is an irrotational velocity field added to satisfy the potential boundary condition, $Up = \nabla\phi$ where $\nabla\phi^2 = 0$ and $\underline{u}.\underline{n} = 0$ on solid boundaries while $\underline{u}.\underline{n} = U$ at the inlet, $\underline{n}$ is the normal unit vector. For the confined shear layer, the boundary condition at x = 0 is: u = U1 for y is greater than 0 and u = U2 for y less than 0, while at y = 0

there is a vortex sheet of strength $\Delta U = U1 - U2$.

In this case, we use Rankine vortex elements, i.e., the vorticity of an element is constant within the core and zero outside, $f(r) = 1/\pi$ for $r < \delta$ and $f(r) = 0$ for $r > \delta$. Correspondingly, $k(r) = r^2/2\pi$ for $r < \delta$ and $k = 1$ for $r > \delta$. Moreover, the potential velocity field is obtained by conformal transformation. Thus, the physical plane is mapped onto the upper half plane and image vortices are used to satisfy the potential boundary conditions. The form of the mapping function for the confined shear layer is given by Ghoniem and Ng (1986).

The motion of the vortex elements must be constructed such that the vorticity field satisfied Equation (1). This is accomplished by solving this equation in two fractional steps:

$$\text{convection:} \quad \frac{\partial \omega}{\partial t} + \underline{u} \cdot \nabla \omega = 0 \tag{7}$$

$$\text{diffusion:} \quad \frac{\partial \omega}{\partial t} = \frac{1}{Re} \nabla^2 \omega \tag{8}$$

In the first step, the convective transport of vorticity is implemented in terms of the Lagrangian displacement of the vortex elements using the current velocity field computed from Equation (6). In the second step, the solution of the diffusion equation is simulated stochastically by the random walk displacement of the vortex elements according to the appropriate population. Thus,

$$\underline{X}i\ (t + \Delta t) = \underline{X}i(t) + \sum_{k} \underline{u}(\underline{X}i_k)\ \Delta t + \underline{\eta}i \tag{9}$$

for $i = 1,2,\ldots,N$, where $\sum$ is a k-th order time-integration scheme and ηi is a two-dimensional Gaussian random variable with zero mean and standard variation

$\sqrt{2\Delta t/Re}$. For more details, see Ghoniem and Ng (1986), Ghoniem and Gagnon (1986).

The no-slip boundary condition at the walls is satisfied by generating new vortex elements to cancel the induced velocity by the vorticity field. Here, we generate vorticity only at the point of separation, i.e., at the tip of the splitter plate, since the growth of the boundary layers along the channel walls at these high Reynolds numbers is small. At each time step, the new vorticity $\Delta T = -\Delta U U_m \Delta t$, where $Um = (U1 + U2)/2$, is consigned to No elements of strength $\Delta T/No$ and added to the field at points $\Delta x = Um\Delta t/No$ apart downstream of $x = 0$ (Figure 1).

The effect of the numerical parameters on the accuracy of the results was investigated by Ghoniem and Ng (1987). Their results emphasized the importance of using a high order time-integration scheme with k=2 to avoid excessive numerical diffusion in the vorticity field. The value of No = 6 was also found to be appropriate, in order to obtain well-defined eddy structures after the rollup and the first two pairings. The second pairing is accomplished within the domain of $0 \leq x \leq 6$, therefore, the computational domain was limited to Xmax = 6. Downstream of Xmax, the vorticity was deleted. Varying Xmax showed that the effect of deleting the vortex elements propagates about one channel height upstream, hence, the results are accurate only for $x \leq 5$.

Flow Structure

To address the capabilities of the vortex method, from flow visualization point of view, the results of some sample simulations are presented in this section.

Results of a typical simulation, presented in terms of the velocity and location of all vortex elements used in the computations, are shown in Figures

2, 3 and 4 for the cases of Re = 24000, Re = 4000, and Re = 1000, respectively. Each vortex element is depicted by a point, while its velocity relative to the mean velocity is represented by a line vector starting at the center of the vortex element. The velocity ratio across the layer at the inlet is U2/U1 = 1/3.

Results show the formation of large vortex eddies by the rollup of the vorticity layer that emanates at the splitter plate and the subsequent pairings of these eddies into larger structures. The rollup of the shear layer was investigated in Ghoniem and Ng (1986) by analyzing results at a wide range of the Reynolds number and at different boundary conditions. Their analysis show that: (1) the rollup is due to the growth of perturbations by the Kelvin-Helmholtz instability mechanism, and the shedding frequency corresponds to the most unstable frequency predicted from the linear stability analysis of a spatially growing layer, (2) pairing, which is associated with the local subharmonic perturbations, results in a step-wise increase in the size of the vorticity layer as two eddies merge, (3) the two sources of the subharmonic perturbations are the downward motion of the layer and the monotonic growth in the size of the eddies downstream, (4) the intrinsic dynamics of the instability is not strongly affected by the value of the Reynolds number, except that at the low Reynolds number the eddies are slightly larger due to the dispersion of vorticity by diffusion, and (5) the computed velocity statistics show good agreements with experimental data, indicating that the fundamental mechanisms of the shear layer are two-dimensional and, hence, the numerical scheme is capable of predicting the large scale features accurately.

3. IMPROVED VORTEX METHODS

Despite the encouraging results obtained by vortex methods in exhibiting the large scale features of the unstable shear layer, it has been recently

found that using a fixed number of vortex elements can lead to large errors in such approaches (Ghoniem et al. 1987a). These errors are mainly caused due to the strong strain field that develops and acts to distort the original vorticity contours. Analysis of the convergence properties of inviscid vortex methods has revealed that the ratio of the core radius to the separation between vortex elements is a major factor in governing the accuracy of vortex computations (Chorin, 1973; Hald, 1979; and Beale and Majda, 1982). Another factor influencing the accuracy are the form of the core function and the scheme of discretizing the initial vorticity.

Figures 2, 3, and 4 clearly show that as the magnitude of the strain rate increases, due to the rollup of the unsteady shear layer, the separation distance within the vortices increases. Considering the fact that these calculations are based on a fixed number of elements with invariant core sizes, this may result in large errors. Large local strains are created, which would lead to strong plane stretch of the vorticity and would cause the initial circular patch of vorticitiy to deform into elliptical, or more complex, shapes with their major axes aligned with the principle direction of the strain field. If the number of computational elements that maintain their original shapes is used, they would not be able to accommodate these severe changes, and this problem may threaten the long-time behavior of the method. Using a large number of elements to discretize the initial patch of vorticity, these elements will naturally migrate in the proper direction, i.e., direction of high strain, and complex formation will arise without the need to modify the cores of individual elements. However, that may necessitate the use of a prohibitively large number of elements initially, or doing a series of runs while increasing the number of elements to guarantee the presence of enough elements after the development of the large strain field until a convergent solution is obtained.

In another work, Ghoniem et al. (1987b) show that using extra elements in the direction of local stretch is a good way of preserving the accuracy. When the distance between two neighboring elements in the direction of principle strain exceeds a minimum value, a new element is placed between the two. This procedure should be done in such a way that the total circulation is conserved and the vorticity distribution is not strongly perturbed. In the simplest form, one may replace the two vortex elements on a line by three elements along the same line (Figure 5a). This, obviously, might result in an excessive number of computational elements within the domain of interest. To remedy this, one may similarly extract elements and combine the two neighboring elements if their separating distance decreases below a critical minimum value (Figure 5b). The critical values for the distance between the neighboring elements to require the injection of a new element, or to combine the two elements into a single one, determines the accuracy of the calculations and is obviously dependent on the computational capabilities. Moreover, this algorithm requires more elaborate programming than conventional vortex methods, since it uses information about neighboring elements in the principle direction of strain (Ghoniem et al., 1987a).

To implement the scheme, we revisited the spatially-evolving flow and distributed the vorticity at the inlet among five layers of vortex elements. This distribution was represented by a Gaussian curve with a spread 2σ:

$$\Omega(x) = \frac{\Delta U}{\sqrt{\pi\sigma}} \exp\left(-\frac{Y^2}{\sigma^2}\right) \qquad (10)$$

which corresponds to an Error function distribution for the velocity.

To ensure the accuracy of discretization of the vorticity among the five layers, it was shown that either a pointwise discretization, $\omega_i = \Omega(X_i)$, or an

area average approach, $\omega_i = \int \Omega(x)\, dx$ (where Xi are the centers of a square mesh of size h) to distribute the vorticity of the shear layer among vortex elements produces large error. Instead, the following scheme was used:

$$\Omega(\underline{X}i) = \sum_{j=1}^{N} \omega_i h^2 \, f_\delta(\underline{X}i - \underline{X}j) \tag{11}$$

where $Ti = \omega_i h^2$ is the circulation of an element of strength ωi, δ is the core radius, and f_δ is the core function. The function $f_\delta(x)$ is written as

$$f_\delta(x) = \frac{1}{\delta^2} f(r/\delta) \tag{12}$$

where

$$r^2 = x^2 + y^2 \tag{13}$$

The function f_δ is radially symmetric, i.e., $\int f_\delta dx=1$ and is a fast decaying function of r/δ so that most of the vorticity is concentrated within $r < \delta$. In the calculations presented below, we used a second order Gaussian core, as suggested by Beale and Majda (1985).

$$f(r) = \frac{1}{\pi} e^{-r^2} \tag{14}$$

In Figure 6, the location and velocity of all the vortex elements are presented. In this figure, the time sequence of the vorticity plot exhibits the large scale features of the flow clearly. In this calculation, the effects of Reynolds number is not taken into account (i.e., inviscid calculations) and the values of α and β (Figure 5) were chosen to be low near the inlet, and to increase linearly with the streamwise direction x. This is described by:

$$\alpha = \alpha_o + \Delta\alpha \; x \tag{15}$$

$$\beta = \beta_o + \Delta\beta \; x \tag{16}$$

For the calculations in Figure 6, $\alpha_o = 2$, $\beta_o = 1$, $\Delta\alpha = 3$ and $\Delta\beta = 2$.

There are no explicit perturbations added onto this flow, and similar to the cases of Figures 2 through 4, the numerical truncation errors are the main reason for perturbing the flow and causing the rollup of the unsteady shear layer. There are approximately 600 vortex elements within the domain and, as can be seen in Figure 6, the initial stages of the development of the unsteady shear layer is not clearly resolved by the selected values of α and β. A finer resolution calculation was performed by decreasing the values of $\Delta\alpha$ and $\Delta\beta$ to 2.5 and 1.5, respectively, while keeping the values of α_o and β_o unchanged. The results of this calculation are presented in Figure 7, and a comparison between this figure and Figure 6 indicates that the structure of large scales of the flow is much more clearly recognizable. In this case, there are about 1000 vortex elements within the computational domain and the simulations required about 45 minutes of cpu time on the Wright-Patterson CRAY-XMP to reach a normalized computational time of $t = 36$. Higher resolution simulation with $\alpha_o = 1.5$, $\beta_o = 0.5$, $\Delta\alpha = 2.5$ and $\Delta\beta = 1.5$ shows the large scale feature of the flow even more clearly. This is presented in Figure 8, where the location and the relative velocities of approximately 2000 elements are shown. Future calculations with better resolution (smaller values of α and β) are recommended to test the dependency of the final results on the process of vortex injections and recombinations. Harmonic perturbations would speed up the processes of the vortex rollup and pairing, as shown in Figure 9. In this figure, the response of the layer, with the same hydrodynamical parameters as that in Figure 6, to the application of the most unstable frequency with low amplitude forcing on the upstream side of the shear layer is presented. The vorticity plots of Figures 6 and 7 indicate that the effect of harmonic forcing is to increase the mixing rate in the initial stages of mixing immediately after the splitter plate, where the resonant eddy is forming. This region is

marked by a row of organized structures, which are created approximately at equal wavelengths from each other due to the application of harmonic forcing (Figure 9) (Browand and Ho, 198[illegible]; Oster and Wygnanski, 1982). At this region, the increased mixing rate results in the augmentation of the chemical reactions (if two reactants were introduced through the two streams of the layer). The results of these calculations are consistent with the previous results of Givi and Jou (1988), who showed that the harmonic forcing plays an important role in the active control of the combustion in the mixing region of the layer if the reaction is assumed to be under equilibrium. What happens for nonequilibrium conditions, when the increased mixing might result in decreased reactions (Givi et al., 1987), cannot be investigated in the present calculations and is the subject of our future investigation.

As mentioned before, a particular advantage of the improved vortex method is in its capability in resolving the regions of high scalar gradients. This superiority can be recognized by a comparison between the vorticity plots in Figures 7 through 9 and those in Figures 2 through 4. This comparison shows that the application of the previously used vortex methods cannot resolve the of high strain, as the vortices tend to evacuate these regions (i.e., braids of the vortices in Figures 2 through 4). The improved vortex method, however, has the advantage that the injection procedure (Figure 5a) prevents the vortices from moving away from the braids and, therefore, allows for the accurate simulations of those regions of the flow field under large local stretch. This feature of the improved vortex method would be particularly useful in diffusion flame calculations where the chemical nonequilibrium effects are most important at regions of high dissipation (strain) rates (Givi et al., 1987, Peters, 1984, Tsuji, 1982, and Liew et al., 1984).

The Transport Element Method

The same philosophy adopted in the vortex methods for the hydrodynamic simulation can be used for the transport of scalar quantities. In such approach, the regions of high scalar gradients may be discretized by transport elements (particles) carrying a certain amount of the gradient of the scalar. This is equivalent to replacing ω and Re in Equation (1) by $Q = \nabla T$ and Pe, where T is a generalized scalar (temperature or concentration) and Pe is the Peclet number. However, as will be seen in this section, contrary to vorticity, the scalar gradients are not conserved along particle path, and their strengths should be modified according to the local stretch and tilting of the material element. To explain this approach, the transport of the conserved scalar quantity, T, is considered

$$\frac{\partial T}{\partial t} + \underline{u} \cdot \nabla T = \frac{1}{Pe} \nabla^2 T \tag{17}$$

using the fractional stepping method, the same as that in Equations (7) and (8), the solution of Equation (17) is equivalent to:

$$\text{Convection} \quad \frac{\partial T}{\partial t} + \underline{u} \cdot \nabla T = 0 \tag{18}$$

$$\text{Diffusion} \quad \frac{\partial T}{\partial t} = \frac{1}{Pe} \nabla^2 T \tag{19}$$

The transport element method is implement by taking the gradient of the Equations (18) and (19)

$$\frac{\partial Q}{\partial t} + \underline{u} \cdot \nabla Q + Q \cdot \nabla u + Q \times (\nabla \times \underline{u}) + \underline{u} \times (\nabla \times Q) \tag{20}$$

$$\frac{\partial Q}{\partial t} = \frac{1}{Pe} \nabla^2 Q \tag{21}$$

The last term in Equation (20) is zero. Since Q is the gradient of a scalar quantity. For a two-dimensional flow, Q can be written as Q = (p, q), where p and q are

$$(q, p) = \left(\frac{\partial T}{\partial x}, \frac{\partial T}{\partial y}\right) \tag{22}$$

In terms of q and p, Equations (20) and (21) become:

$$\frac{\partial q}{\partial t} + \underline{u}\cdot\nabla q = -q\frac{\partial u}{\partial x} - p\frac{\partial v}{\partial x} \tag{23}$$

$$\frac{\partial p}{\partial t} + \underline{u}\cdot\nabla p = -q\frac{\partial u}{\partial y} - p\frac{\partial v}{\partial y} \tag{24}$$

$$\frac{\partial q}{\partial t} = \frac{1}{Pe}\nabla^2 q \tag{25}$$

$$\frac{\partial p}{\partial t} = \frac{1}{Pe}\nabla^2 p \tag{26}$$

The RHS of Equations (23) and (24) indicate that the strength of the scalar gradients (i.e., the magnitude of p and q within each element) would change along the particle path. Therefore, the convective step (Equations 23 and 24) will be completed in two fractional steps:

Pure convection $$\frac{\partial q}{\partial t} + \underline{u}\cdot\nabla q = 0 \tag{27}$$

Source adjustment $$\frac{\partial q}{\partial t} = -q\frac{\partial u}{\partial y} - p\frac{\partial v}{\partial x} \tag{28}$$

A similar procedure would also follow for p.

In the first fractional step (Equation 27), the location of the gradient element changes in a Lagrangian sense, and in the second fractional step the

strength of the gradient is changed to satisfy Equation (28). The magnitude of the gradient at a location x is, then, computed from:

$$\underline{Q}(\underline{x},t) = \sum_{i=1}^{N} Qi(t)h^2 f_\delta\ (\underline{x} - \underline{x}_i) \tag{29}$$

where f is the core function for the transport elements and can be chosen to be different from the vorticity elements. In this work, we used the same core functions (second order Gaussian).

Once the location and the magnitude of the strength of the scalar gradients (p,q) are known, the magnitude of the scalar (T) can be easily obtained by using the Green's function approach as developed by Anderson (1983). According to this method, the solution of the equation

$$\nabla^2 T = \nabla \cdot Q \tag{30}$$

can be written as

$$T = \int (\nabla \cdot \underline{Q})\ G dx \tag{31}$$

where

$$G = -\frac{1}{2\pi} \ln r \tag{32}$$

is the Green function of the Poisson equation. Integration Equation (31) by parts results in:

$$T = \int (\underline{Q} \cdot \nabla G)\ dx \tag{33}$$

Using Eq. (29) for $\underline{Q}$, we have:

$$T(\underline{x},t) = \sum_{i=1}^{N} \underline{Q}i(t) \cdot \nabla G_\delta\ (\underline{x} - \underline{x}_i(t))h^2 \tag{34}$$

where

$$G_\delta = \frac{(x,y)}{r^2}\, k(\frac{r}{\delta}) \qquad (35)$$

and δ is the core function.

This expression is convenient when used in connection with the vortex method because the same elements used in the transport of the vorticity may be used for the scalar gradient transport (when Re = Pe and the same initial boundary conditions). Also, the same injection-recombination procedure as used in the improved-vortex calculations, may be used in the gradient transport simulations to accurately simulate the regions of high scalar gradients. The need for the insertion is more apparent here since the magnitude of the gradient increases where the strain field is high.

To implement the procedure, the transport of a conserved scalar variable with a normalized value of T = 0 in the high speed stream and T = 1 in the low speed stream is considered. The magnitude of the diffusivity of this scalar quantity is assumed zero so that the same vortex elements can be used for the transport of the gradient Q. Calculations were performed for the same hydrodynamical conditions as that presented in Figure 6. Therefore, the vortex plots in this figure would also exhibit the gradients plots in that the locations of the transport elements and those of the vortices coincide. Of course, the strengths of the computational elements would be different in the two cases.

The instantaneous values of the scalar variable T, calculated from Equation (34) are statistically analyzed for the purpose of comparison with experimental data. This analysis was performed by averaging the instantaneous values at every time step during the period $t1 \leq t \leq t2$. The vlaue of t1 was

selected as twice the value of the residence time t1 = 2xmax/Um, so that the effects of initial transients are washed out of the domain. The period of ΔT = t1-t2 was selected as four times the value of the residence time (i.e., ΔT = 4Xmax/Um), so that it is large enough for the purpose of statistical analysis. During this period an ensemble of 160 data points was gathered that resulted in almost identical statistics to those with an ensemble of 80 sample data points. Therefore, higher ensemble sizes were not considered to minimize the computational costs.

The mean and rms values of the scalar variable T are presented in Figures 10 and 11 versus the reduced coordinate, η = (Y-Yo)/(X-Xo), where Yo is measured at $\overline{T}$ = 0.5 ($\overline{\ }$ indicates the ensemble average) and Xo is the virtual origin of the mixing layer based on the mean scalar profile (in this simulation, Xo = 0). In these figures, the solid lines are the results of simulations and the data points are obtained from the experimental measurements of Masutani and Bowman (1986) for a dilute nonreacting mixing layer with the same velocity ratio. It is evident from these two figures that both the mean and the rms of the passive scalar are accurately predicted across the width of the shear layer. It is particularly encouraging to note that both these profiles are in better agreement with data than those obtained previously by Givi et al. (1985) utilizing a K-ε turbulent model and a gradient diffusion model of turbulent transport of the scalar mean, moments and PDF (probability density function). In particular, the K-ε model was not capable of accurately predicting the behavior of the scalar field near the high speed stream where the effects of large scale structures are important. The effects of intermittency, which are not included in the K-ε calculations, are explicitly accounted for in the present simulations (Figures 6 through 9) and allow for better comparison with data near the high speed stream. Moreover, the

simulations indicate the presence of two local maxima in the rms profiles that correspond approximately to the locations where the gradient of the mean value is highest, as also indicated in the results of Masutani and Bowman (1986) and Batt (1977). In view of these comparisons with data, it is clear, in accordance with the findings of Broadwell and Briedenthal (1982), that the intermittency caused by the large coherent structures contribute greatly to the statistics of this unsteady flow.

The probability density functions (PDF's) of the scalar variable was also constructed from the 160 ensemble data points. The cross stream variation of the PDF's are presented in Figure 12 for the same streamwise location as those in Figures 10 and 11. In this figure, T represents the instantaneous scalar values and the PDF is defined such that

$$P(\tilde{T})\, d\tilde{T} = \text{Prob}\,\{\tilde{T} < T < \tilde{T} + d\tilde{T}\} \qquad (36)$$

In this figure, the delta function at T = 0 indicates the fluid from the high speed stream and the delta function at T = 1 represents the low speed fluid concentration. It is also observed that, as the layer is traversed, the height of the PDF's within the layer represents the fluid in the mixing core. The results presented in this figure are similar to those observed experimentally in the pretransitional regions of the layer (Koochesfahani, 1984). However, they do not agree with the recent studies of Givi and McMurtry (1987) and Givi and Jou (1988), who showed that the mechanisms of the vortex rollup, and the pairing process in particular, contribute greatly to the generation of a third peak (a third delta function) at a mixture concentration whose value depends on the velocity difference across the layer. There are two main reasons for this disagreement. First, in the present calculations, only the convective transport of the scalar is considered and the contributions of the diffusive transport

are taken into account (i.e., infinite Peclet number). The effects of diffusivity are to expand the core of the transport element and, as a result, to mix the fluid better within the mixing region. That may contribute to the generation of the predominant peak of the PDF's. Second, the number of vortex (and transport) elements employed in the present calculations may not be large enough to accurately capture the PDF's, which are "sensitive" statistically even though less sensitive quantities, such as the mean and the rms, are accurately predicted.

Future calculations with larger number of computational elements will be a logical continuation of the present work.

4. CONCLUSION

A Lagrangian numerical scheme based on an improved vortex-transport element method has been employed to investigate the mechanism of mixing in a spatially developing, two-dimensional shear layer configuration. In this scheme, Lagrangian elements are used to transport vorticity and also the gradients of the scalar variables. A particular advantage of this method is that it optimizes the computational efforts by distributing the vortex and the transport elements around the regions of high vorticity and high gradients.

An injection procedure is employed to prevent the computational elements from evacuating the regions of high local stretch. The implementation of this procedure makes this improved method more attractive than the conventional vortex methods in that regions of large dissipation rates (i.e., the braids of the vortices) can be more accurately simulated. The coherent large structures of the flow can be nicely exhibited by "fine tuning" of this injection procedure.

The resulting scheme was utilized to simulate the convective transport of a passive scalar quantity within the mixing region of the layer. The

statistical analysis of the instantaneous results showed favorable agreements with experimental data for the first two moments (mean and rms) of the scalar. However, it seems that to make a better comparison with measured data for the PDF's of the scalar variable, simulations should be performed with larger number of transport elements.

Harmonic perturbation of the velocities at the inlet of the layer was shown to have a significant effect in accelerating the process of the vortex rollup and creating large organized structures within the mixing regions of the flow. This resulted in the convolution of the interphase surfaces and the improvement of mixing in the region immediately behind the splitter partition plate. This would be very important in controlling the outcome of the chemical reactions in combusting shear layer configuration, which would be a logical extention of this work.

Calculations with higher number of transport elements are recommended also for better flow visualizations and to check the sensitivity of the statistical variables on the total number of Lagrangian elements.

REFERENCES

Anderson, C. (1983) Ph.D. Thesis, University of California, Berkeley, CA.

Ashurst, W. T., and Barr, P. K. (1982) Sandia Report *SAND80-9950*.

Batt, R. G. (1977) J. Fluid Mech., Vol. 82, pp. 53-95.

Beale, J. T., and Majda, A. (1982) Math. Comput., Vol. 39, pp. 29-52.

Beale, J. T., and Majda, A. (1985) J. Comp. Physics, Vol. 58, p. 188.

Bilger, R. W. (1976) Prog. Energy and Combust. Sc., Vol. 1, pp. 87-109.

Bilger, R. W. (1980) Turbulent Reacting Flows, Springer-Verlag, Berling, pp. 65-113.

Broadwell, J. E., and Breidenthal, R.E. (1982) J. Fluid Mech., Vol. 125, pp. 397-410.

Browand, F. E., and Ho, C.-M. (1983) Journal de Mecanique theorique et Appliquee Numero Special, pp. 99-120.

Chorin, A. J. (1973) J. Fluid Mech., Vol. 57, pp. 785-796.

Corcos, G. M., and Sherman, F. S. (1984) J. Fluid Mech., Vol. 139, pp. 29-65.

Donaldson, C. duP., and Varma, A. K. (1976) Combust. Sci. and Tech., Vol. 13, pp. 55-78.

Ghoniem, A. F. (1986) Lectures in Applied Mathematics, Vol. 24, pp. 199-265.

Ghoniem, A. F., Chorin, A. J., and Oppenheim, A. K. (1982) Phil. Trans. R. Soc. Lond., Vol. A304, pp. 303-325.

Ghoniem, A. F., and Gagnon, Y. (1986) J. Comput. Phys., Vol. 68, in press (1987) and AIAA Paper No. 86-0370.

Ghoniem, A. F., and Givi, P. (1987) AIAA Paper 87-0225.

Ghoniem, A. F., Heidarienejad, G., and Krishnan, A. (1987a) J. Comput. Phys., submitted for publication.

Ghoniem, A. F., Heidarienejad, G., and Krishnan, A. (1987b), presented at AIAA/SAE/ASME/ASEE 23rd Joint Conference, San Diego, CA, June 29-July 2.

Ghoniem, A. F., and Ng, K. K. (1986) AIAA Paper No. 86-0056.

Ghoniem, A. F., and Oppenheim, A. K. (1984) AIAA Journal, Vol. 22, 10, pp. 1429-1435.

Ghoniem, A. F., and Sherman, F. S. (1985) J. Comput. Phys., Vol. 61, pp. 1-37.

Givi, P. (1984), Ph.D. Thesis, Carnegie Tech., Pittsburgh, PA.

Givi, P., and Jou, W.-H., (1988) Journal of Non-Equilibrium Thermo., in press.

Givi, P., and McMurtry, P. A. (1988) Combust. Sci. Tech., Vol. 57, 4-6, p. 141.

Givi, P., Jou, W.-H., and Metcalfe, R. W. (to appear) Proceedings of 21st Symposium (International) on Combustion, The Combustion Institute, Pittsburgh, PA.

Givi, P., Ramos, J. I., and Sirignano, W. A. (1984a) AIAA Prog. Astron. and Aeron., Vol. 95, pp. 384-448.

Givi, P., Ramos, J. I., and Sirignano, W. A. (1985) Journal of Non-Equilibrium Thermodynamics, Vol. 10, No. 2, pp. 75-104.

Givi, P., Sirignano, W. A., and Pope, S. B. (1984b) Combust. Sci. Tech., Vol. 37, pp. 599-74.

Grinstein, F. F., Oran, E. S., and Boris, J. P. (1985) NRL Memorandum Report 5621, Washington, D.C., also J. Fluid Mech., Vol. 165, pp. 201-220.

Hald, O. (1979) SIAM J. Numer. Anal., Vol. 22, pp. 726-755.

Koochesfahani, M. M. (1984) Ph.D. Thesis, Calif. Inst. of Technology, Pasadena, CA.

Liew, S. K., Moss, J. B., and Bray, K. N. C. (1984) AIAA Prog. in Astron. and Aeron., Vol. 95, pp. 305-319.

Lin, P., and Pratt, D. T. (1987) AIAA Paper No. 87-0224.

Lockwood, F. C., and Naguib, A. S. (1975) Combust. Flame, Vol. 24, pp. 109-124.

Masutani, S. M., and Bowman, C. T. (1986) J. Fluid Mech., Vol. 172, pp. 93-126.

McMurtry, P. A., Jou, W.-H., Riley, J. J., and Metcalfe, R. W. (1986) AIAA Journal, Vol. 24, Number 6, pp. 962-970.

Nguyen, T. V., and Pope, S. B. (1984) Combust. Sci. Tech., Vol. 42, pp. 13-45.

Oran, E. S., and Boris, J. P. (1987) Numerical Simulation of Reactive Flows, Elsevier Science Publishing Co.

Oster, D., and Wygnanski, I. (1982) J. Fluid Mech., Vol. 123, pp. 91-130.

Peters, N. (1984) Prog. Energy Combust. Sci., Vol. 10, pp. 319-339.

Pope, S. B., and Correa, S. M. (1987) Proceedings of 21st Symposium (International) on Combustion, Combustion Institute, Pittsburgh, PA.

Riley, J. J., Metcalfe, R. W., and Orszag, S. A. (1986) Phys. Fluids, Vol. 29, pp. 406-422.

Sethian, J. A. (1984) J. Comput. Phys., Vol. 54, 3, pp. 425-456.

Tsuji, H. (1982) Prog. Energy Combus. Sci., Vol. 8, p. 93.

Acknowledgement

The calculations reported here are based on the modifications of the computer codes originally developed by Ghoniem et al. (1987a, 1987b). The author wishes to acknowledge Drs. Ahmed Ghoniem and Ghasem Heidariengejad for valuable discussions.

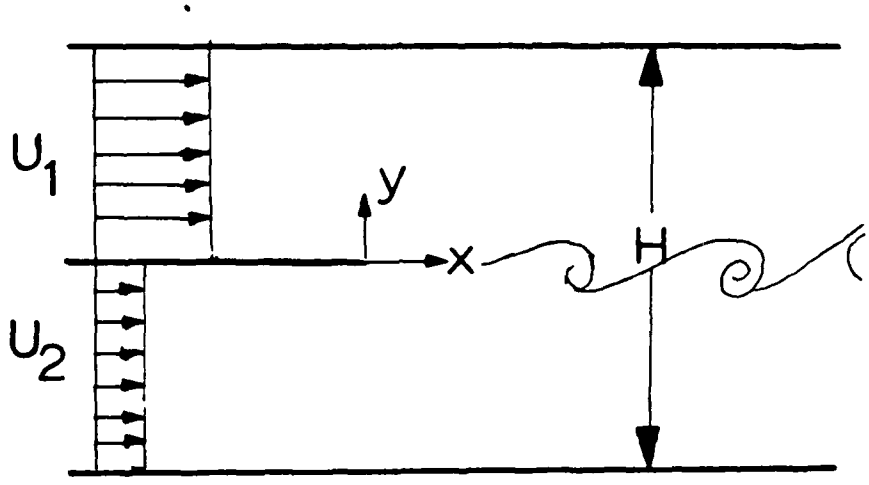

Figure 1. Geometrical configuration.

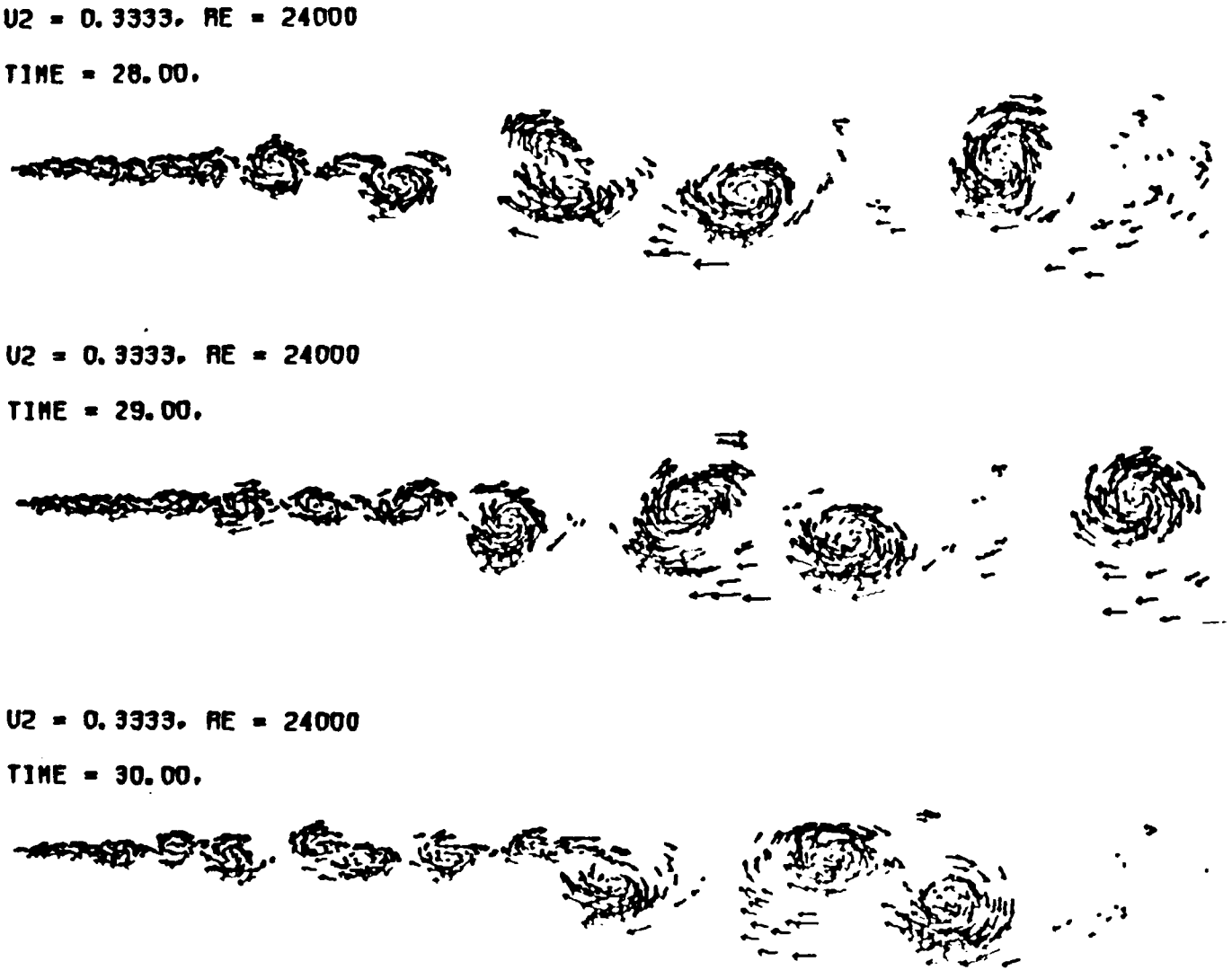

Figure 2. Vorticity field at Re = 24000 and U_2/U_1 = 1/3 by vortex method. The splitter plate is located on the left side of the figure.

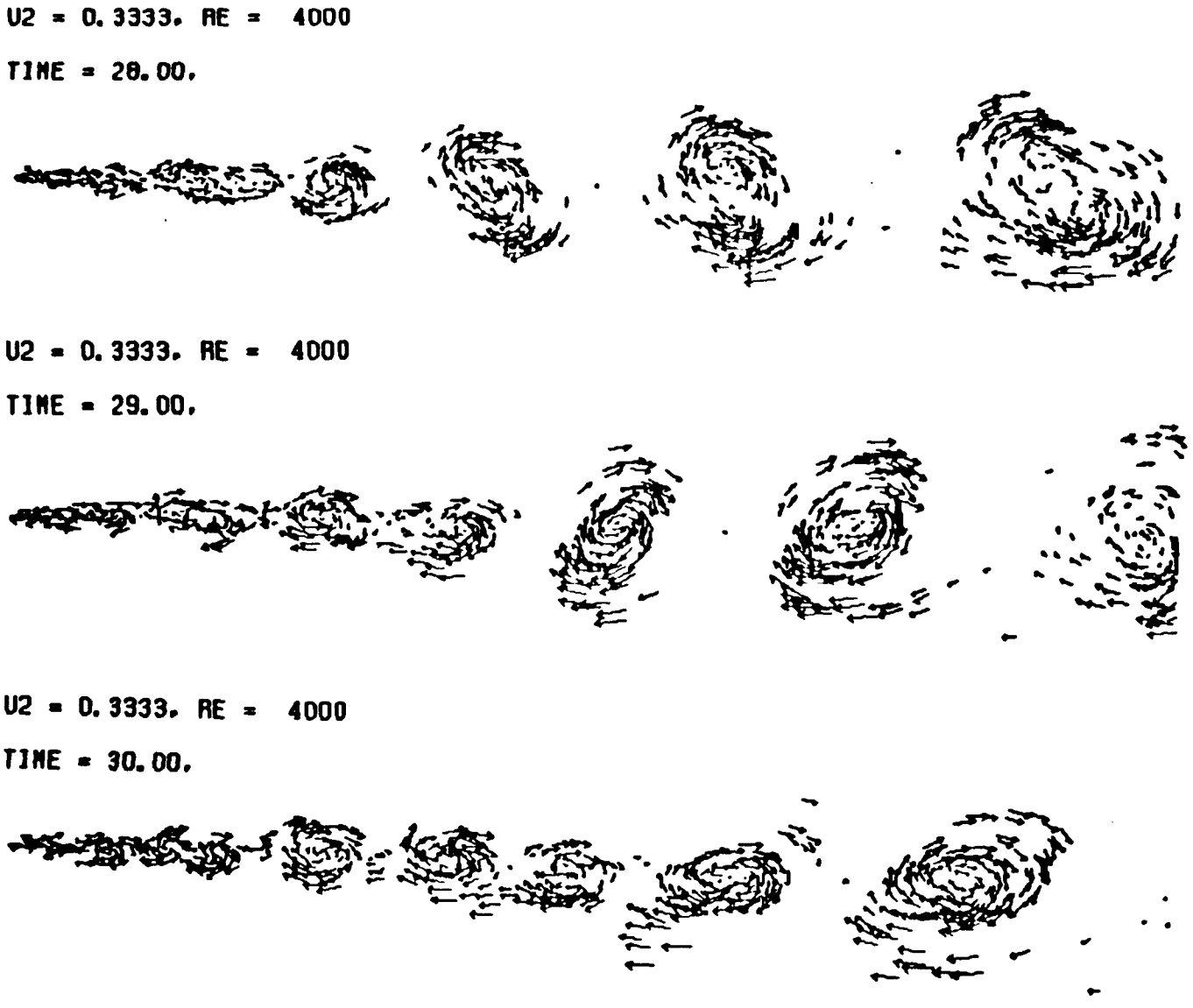

Figure 3. Vorticity field at Re = 4000 and U_2/U_1 = 1/3 by vortex method. The splitter plate is located on the left side of the figure.

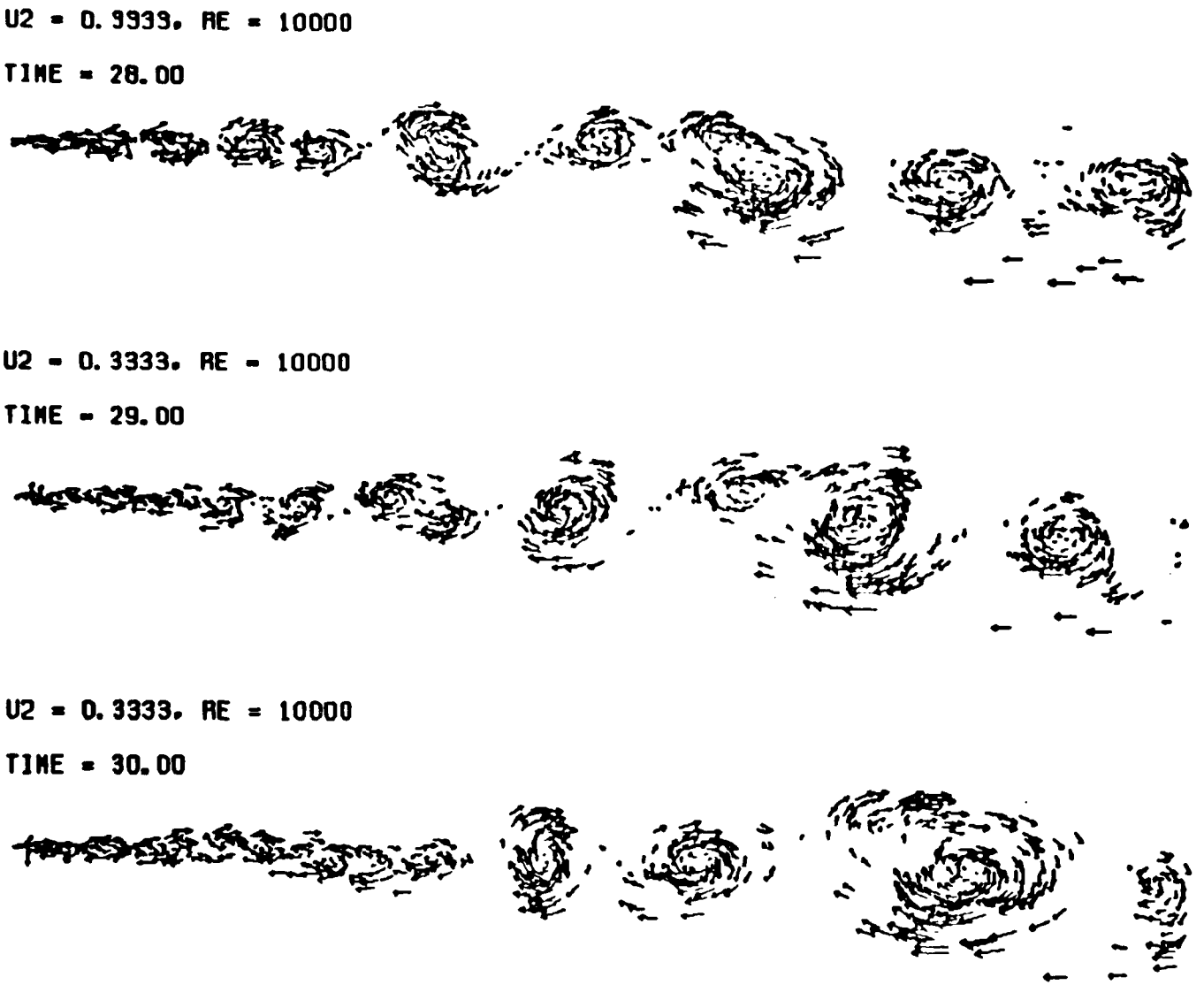

Figure 4. Vorticity field at Re = 1000 and U_2/U_1 = 1/3 by vortex method. The splitter plate is located on the left side of the figure.

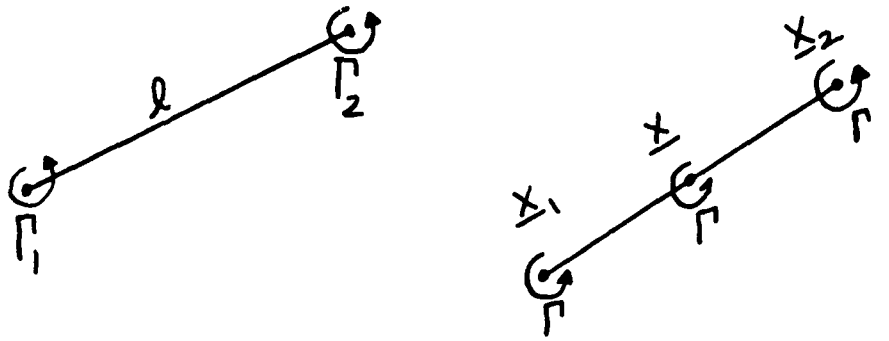

$$\ell > \alpha h$$
$$\Gamma = (\Gamma_1 + \Gamma_2)/3$$
$$\underline{X} = (\underline{X}_1 + \underline{X}_2)/2$$

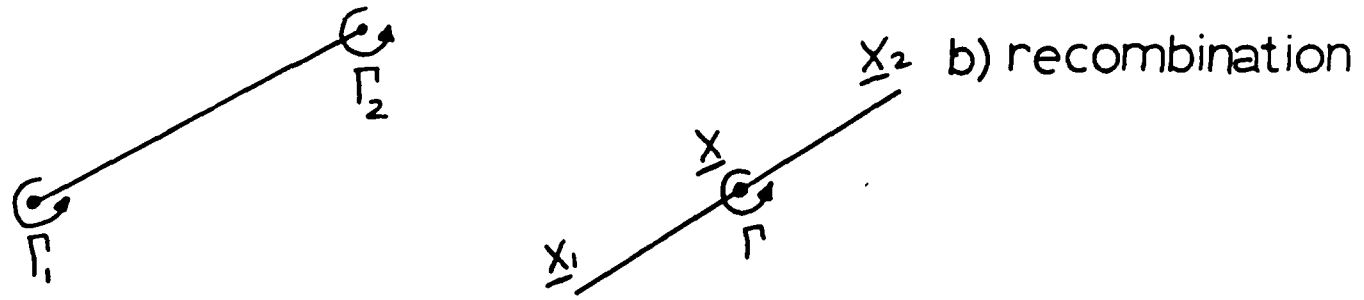

$$\ell < \beta h$$
$$\Gamma = (\Gamma_1 + \Gamma_2)$$
$$\underline{X} = (\underline{X}_1 + \underline{X}_2)/2$$

Figure 5. Injection and recombination mechanisms in improved vortex method.

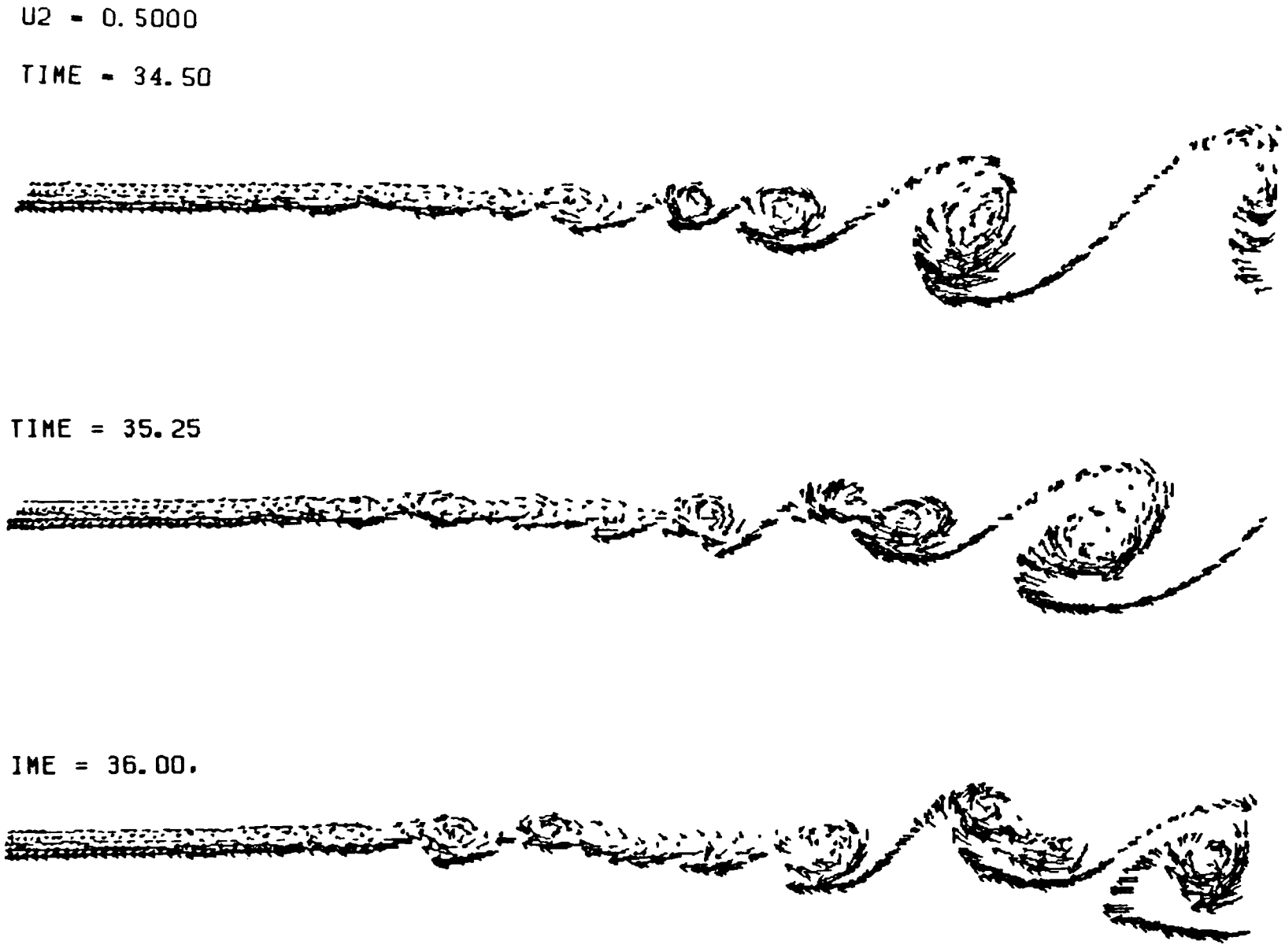

Figure 6. Vorticity field by improved vortex method. Inviscid calculations. The splitter plate is located on the left side of the figure. $\alpha_0 = 2$, $\beta_0 = 1$, $\Delta\alpha = 3$, $\Delta\beta = 2$.

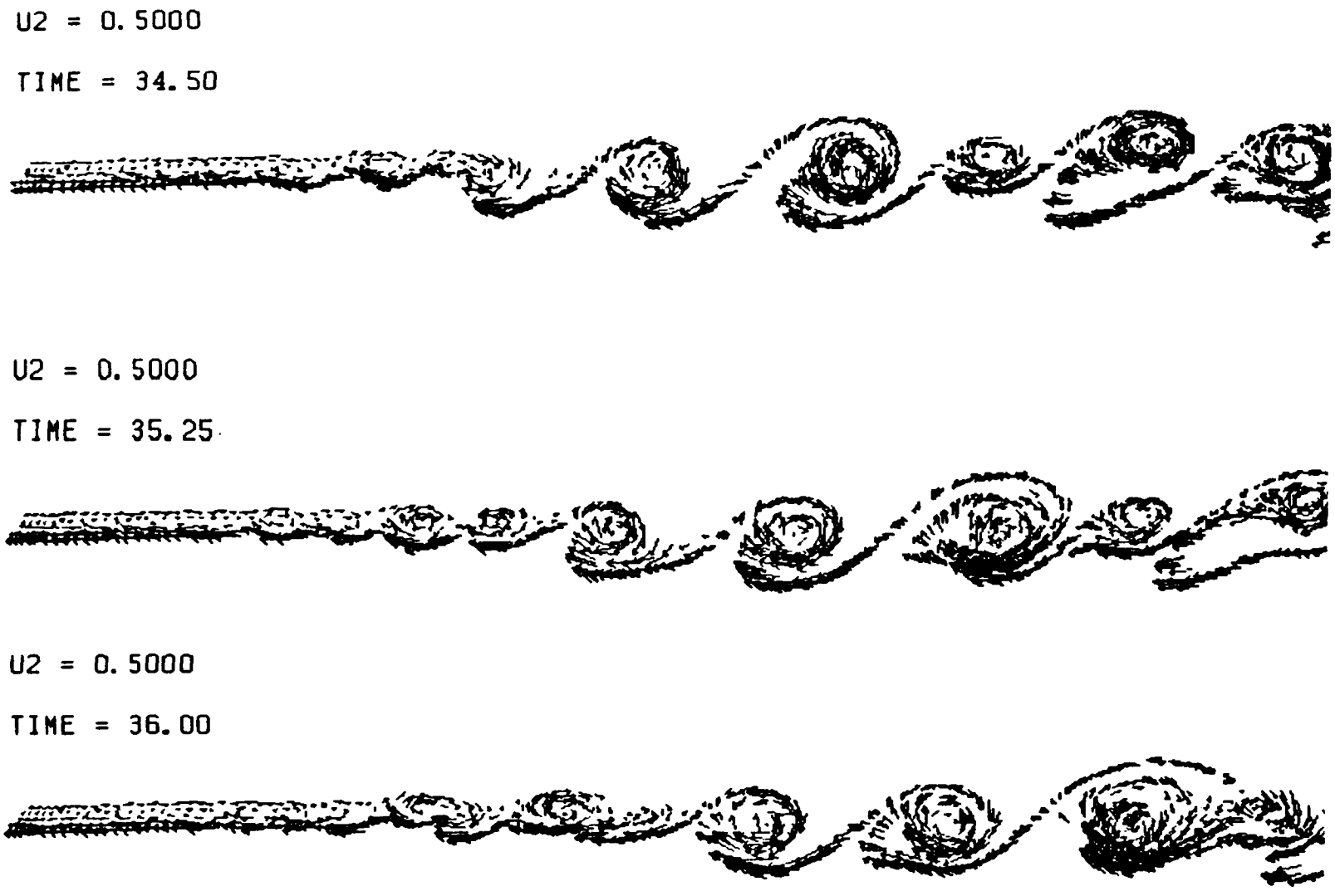

Figure 7. Vorticity field by improved vortex method. Inviscid calculations. The splitter plate is located on the left side of the figure. $\alpha_0 = 2$, $\beta_0 = 1$, $\Delta\alpha = 2.5$, $\Delta\beta = 1.5$.

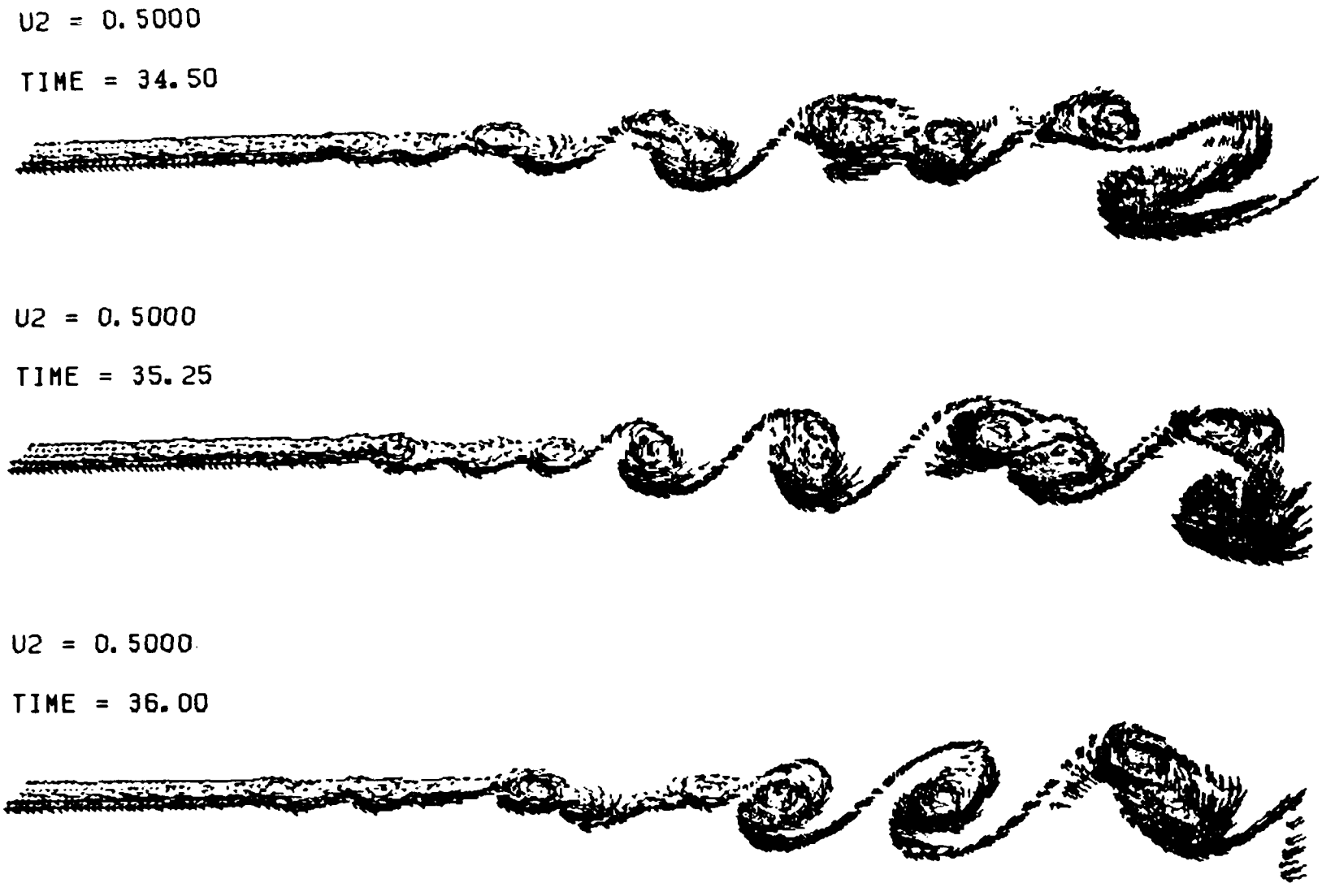

Figure 8. Vorticity field by improved vortex method. Inviscid calculations. The splitter plate is located on the left side of the figure. $\alpha_0 = 1.5$, $\beta_0 = 0.5$, $\Delta\alpha = 2.5$, $\Delta\beta = 1.5$.

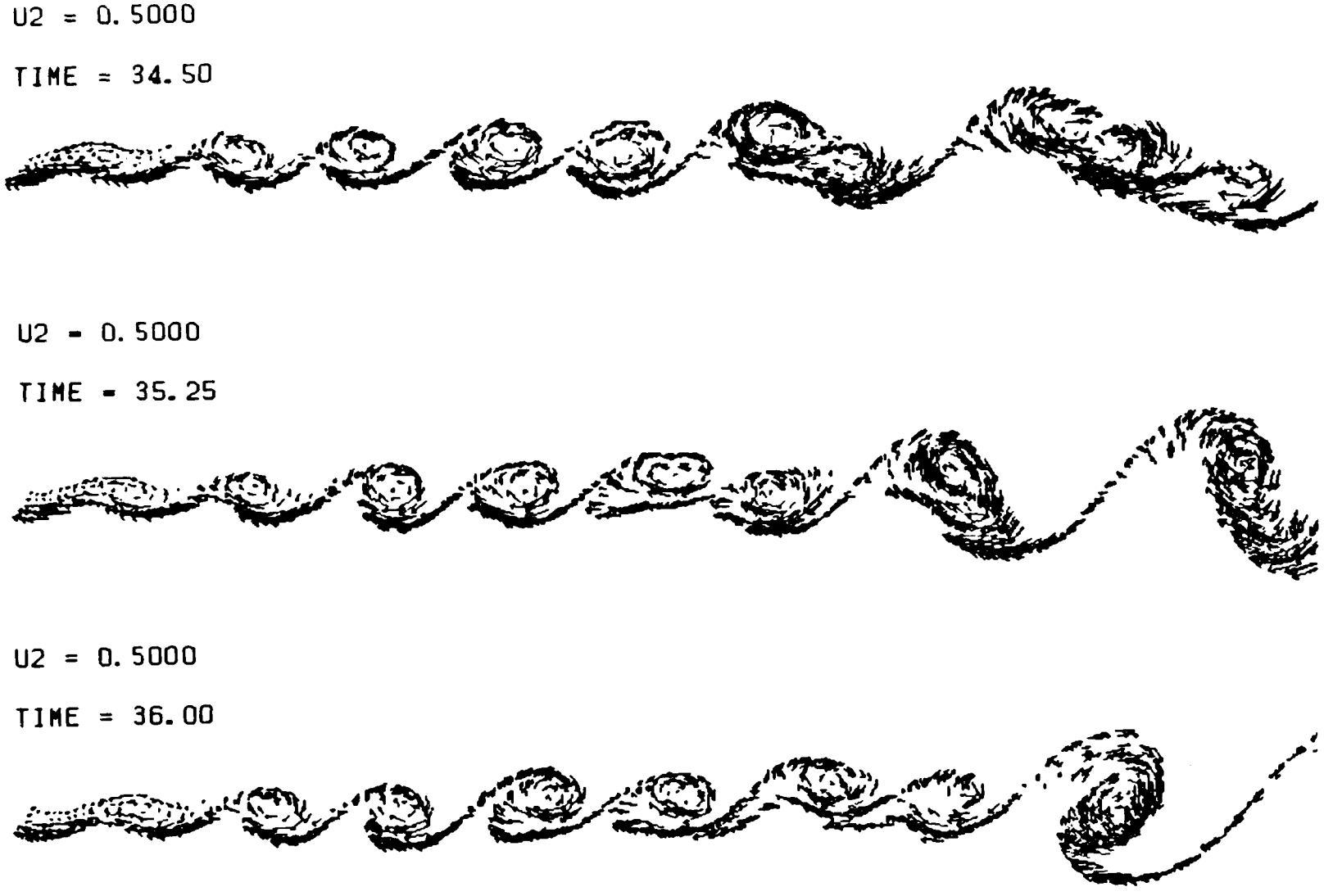

Figure 9. Vorticity field by improved vortex method. Inviscid calculations. Harmonically forced layer at the same conditions as in Figure 6. The splitter plate is located on the left side of the figure.

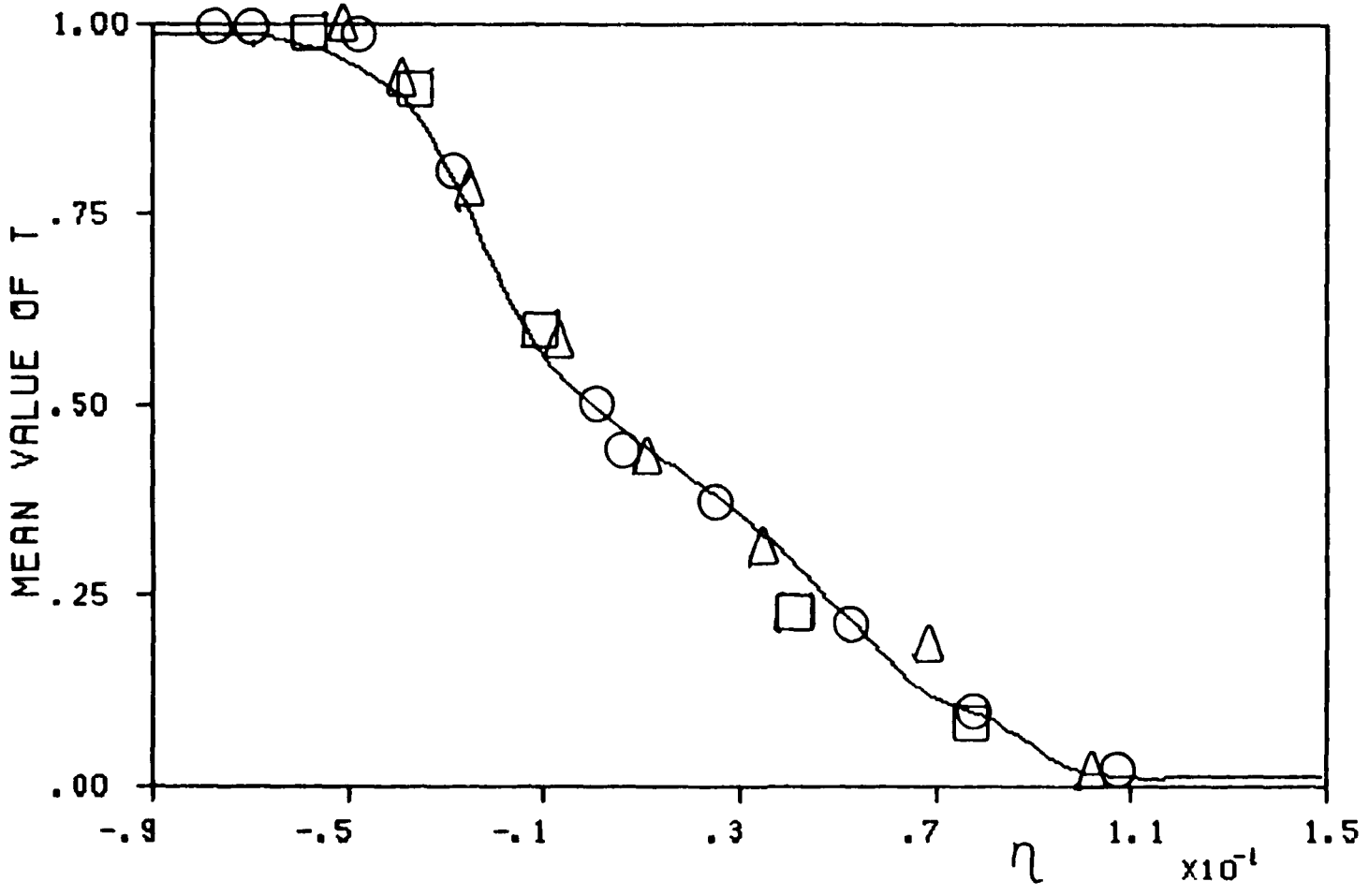

Figure 10. Mean scalar profile vs. the cross-stream coordinate. ⌒, present simulations; O , Δ , □ , experimental data obtained by Masutani and Bowman (1986) at different stream-wise locations.

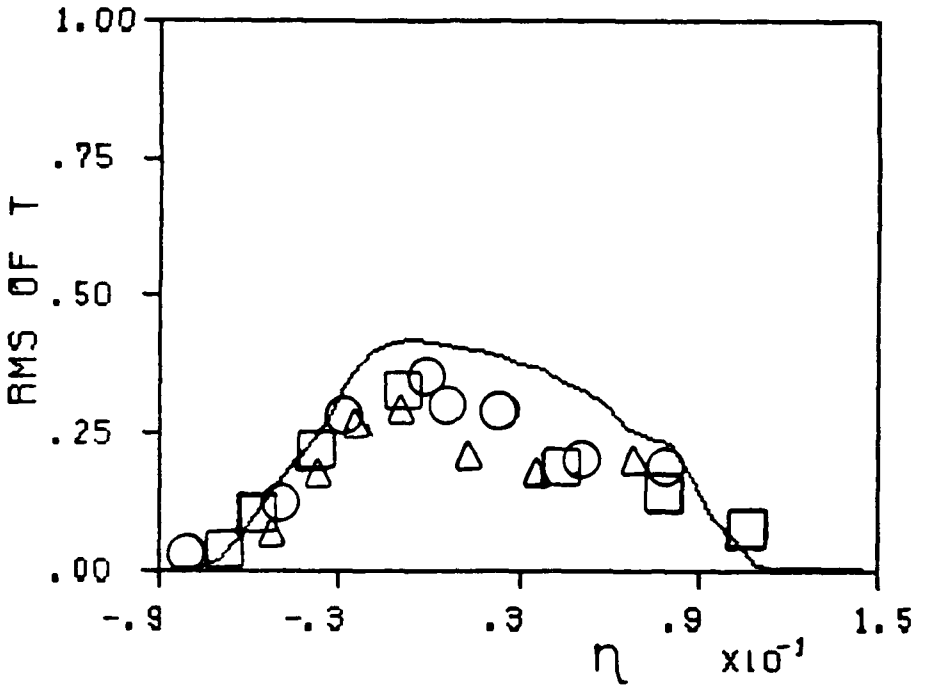

Figure 11. Rms scalar profile vs. the cross-stream coordinate. ⌒, present simulations; 0 , Δ , □ , experimental data obtained by Masutani and Bowman (1986) at different stream-wise locations.

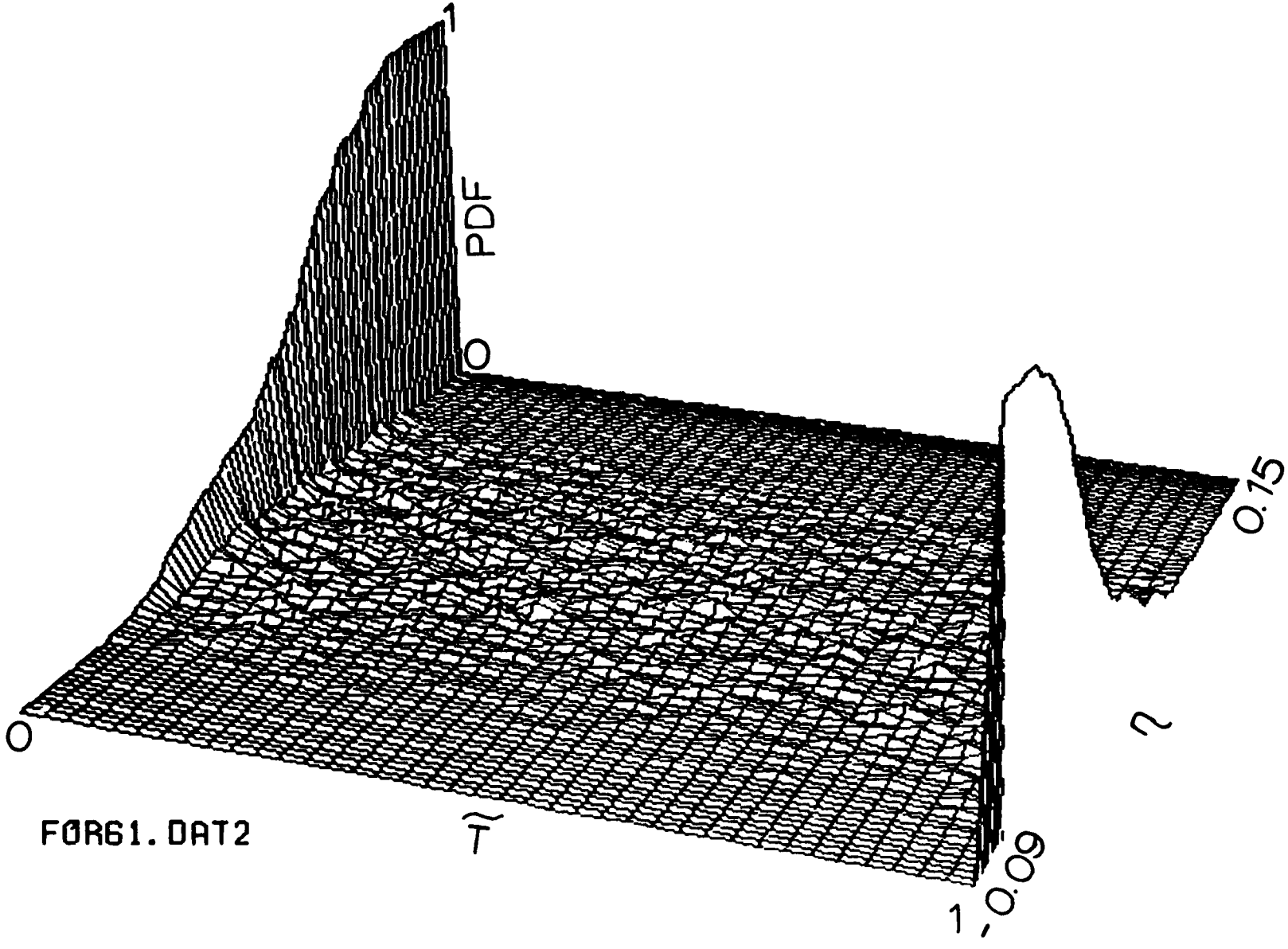

Figure 12. PDF's scalar vs. the scalar space and the cross-stream coordinate.